Photonic shape memory chiral nematic polymer coatings with changing surface topography and color

ADVANCED OPTICAL MATERIALS
www.advopticalmat.de

Photonic Shape Memory Chiral Nematic Polymer Coatings with Changing Surface Topography and Color

*Koen Nickmans, Danielle A. C. van der Heijden, and Albert P. H. J. Schenning**

The fabrication of shape memory coatings that change both reflectivity and topography is hampered by the lack of facile methods and materials. Now, shape memory photonic coatings are fabricated by high-speed flexographic printing and UV-curing in air of a chiral nematic liquid crystal ink. Deformable polymeric films with a red reflection band and a smooth surface topography are obtained which can be thermally programmed above room temperature by using a rough stamp. This thermomechanical programming results in a temporary rough surface topography leading to surface scattering and as a result a gray color below room temperature. By heating the coatings, a shape recovery to the permanent state is observed, thereby restoring the smooth surface topography and the iridescent red reflection color. It is shown that this recovery is highly temperature dependent, which allows for a fast and distinct optical and topography change upon exceeding room temperature. These thermoresponsive photonic crystal coatings have a great potential as low-cost optical sensors, smart adhesives, and adaptive biosurfaces.

1. Introduction

Shape memory polymers (SMPs) which can be deformed into a temporary shape and subsequently recovered into a permanent memorized shape via external stimuli are receiving a lot of attention.[1–4] Such polymers can also be used as coatings capable of changing their surface topography.[5–9] These smart surfaces have been fabricated, for example, by thermomechanical programming at biologically relevant temperatures[10] for dynamic control of adhesion,[11,12] wetting of liquids,[13] and cell–topography interactions.[14,15]

SMP coatings that change both topography and color are appealing for a range of reconfigurable nanophotonic devices for optical data storage, photovoltaics,[16] and optical sensors,[17,18] as well as smart adhesives,[19] biosurfaces,[20] and battery-free optical time-analyte indicators.[21,22] Regular surface topographies exhibiting structural colors have been fabricated in SMPs by top-down methods including locally induced surface wrinkling,[23] nanoimprint lithography,[24,25] compression molding,[26] or templating via microspheres.[27] In these examples, hot pressing of the surface features results in a temporary flattened and colorless state, which is reversible upon heating.[24–27]

To circumvent the cumbersome top-down nanoforming steps to generate the structural color, photonic SMP coatings generated by bottom-up self-assembly have also been employed.[17,28,29] For example, shape memory photonic films have been produced from core–interlayer–shell polymer microspheres that form opal structures.[30–32] Alternatively porous inverse-opal SMPs have been templated by silica colloids.[33] Capillary pressure-induced "cold" programming of these materials results in a disordered temporary state consisting of collapsed pores and an arbitrarily roughened surface, which can be recovered by pressure, heat, organic vapors, solvents, and microwave radiation.[34–39] Unfortunately, the fabrication of such SMP coatings is still hampered by the lack of facile methods and materials.[40]

Reactive liquid crystalline materials are exciting from this perspective since they form nanostructured phases via self-assembly, and can be easily processed via photopolymerization[41–44] to fabricate polymeric coatings.[45–49] Chiral nematic liquid crystalline (a.k.a. cholesteric liquid crystalline (CLC)) phases are of particular interest for their periodic helical structures which lead to the selective and incident-angle-dependent reflection of light, resulting in iridescent structural colors.[50] CLC coatings have been reported that respond to stimuli including heat, light, and humidity.[17,51–57] In addition, CLC coatings have been reported that simultaneously change surface topography and color in a reversible manner.[41,55]

Recently, our group reported that irreversible thermoresponsive photonic coatings can be fabricated based on CLC polymer networks using a shape memory approach.[58,59] Indentation of a small area (≈1 mm^2) of the CLC film, at a temperature above the T_g of the polymer network, resulted in a blue-shift of the reflection band through a reduction of the pitch of the cholesteric helix, which was fully recovered upon heating.

We now report a new approach for the fabrication of shape memory photonic coatings that irreversibly change both topography and color. Polymeric CLC films with a red structural

Dr. K. Nickmans, D. A. C. van der Heijden, Prof. A. P. H. J. Schenning
Laboratory of Stimuli-responsive Functional Materials and Devices
Department of Chemical Engineering and Chemistry
Eindhoven University of Technology
P.O. Box 513, 5600 MB, Eindhoven, The Netherlands
E-mail: a.p.h.j.schenning@tue.nl

The ORCID identification number(s) for the author(s) of this article can be found under https://doi.org/10.1002/adom.201900592.

DOI: 10.1002/adom.201900592

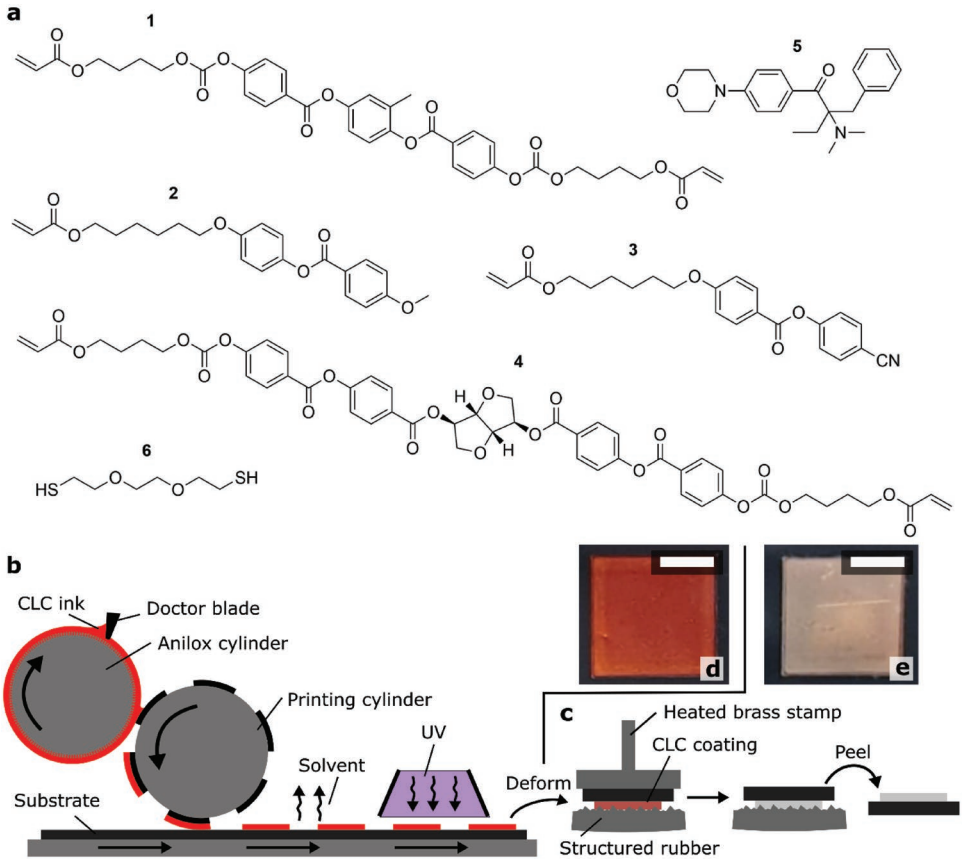

Figure 1. a) Molecular structures of used chemicals. b) Schematic fabrication protocol via flexographic printing and UV-curing of cholesteric liquid crystal ink. c) Schematic deformation protocol consisting of pressing the CLC coating into a structured rubber using a heated brass stamp and subsequently peeling it off of the rubber. d) Photograph of photonic coating on a black PET substrate. e) Photograph of a photonic coating after deformation. Scale bar = 1 cm.

color and a smooth surface topography are obtained by high-speed flexographic printing and UV-curing in air of a chiral nematic liquid crystal ink. These coatings can be thermally programmed by using a rough stamp resulting in a temporary rough surface topography leading to scattering and a gray color below the glass transition temperature which is at room temperature. By heating the coatings, a total shape recovery to the permanent state is observed, thereby restoring the smooth surface topography and the iridescent red reflection color. It is shown that this recovery is highly temperature dependent, which allows for a fast and distinct optical response upon exceeding the glass transition temperature. Our approach allows the facile fabrication of thermoresponsive photonic coatings of commercially relevant dimensions with an easily perceived color and surface topography change at biologically relevant temperatures using highly scalable fabrication methods.

2. Results and Discussion

For the fabrication of shape memory CLC coatings, we designed a reactive liquid crystal mixture that is composed of a difunctional crosslinker **1**, monofunctional acrylates **2** and **3**, chiral dopant **4**, photoinitiator **5**, and a difunctional thiol **6** (**Figure 1**a). The thiol acts as an oxygen inhibitor thereby allowing photopolymerization in air,[60] and as a chain extender via radical thiol-acrylate polymerization, thereby reducing the crosslinking density and lowering the T_g to room temperature (vide infra).[61] The composition of the mixture was chosen such that a red reflective, deformable coating was obtained, but in principle any color is possible by varying the chiral dopant concentration.[18,51] Thermal characterization of the mixture by polarized optical microscopy (POM) and differential scanning calorimetry (DSC) showed a room temperature chiral nematic phase, characterized by a typical Schlieren defect texture (Figure S1, Supporting Information). The chiral nematic to isotropic (N*–I) transition was situated around 50 °C upon heating, but upon cooling suppressed to around 25 °C and less well-defined, likely due to the relatively high amount of non-mesogenic material present. The mixtures did not crystallize on the timescale of the DSC measurement (>1 h). Therefore, the mixtures can be printed and annealed at room temperature, without the risk of crystallization prior to photopolymerization.

Polymeric photonic coatings were prepared using flexographic printing (Figure 1b).[62] A printing ink was prepared by adding a compatible solvent (cyclopentanone) and a small amount (0.1 wt%) of surfactant[63] to promote planar alignment at the coating–air interface. The ink was deposited on an anilox

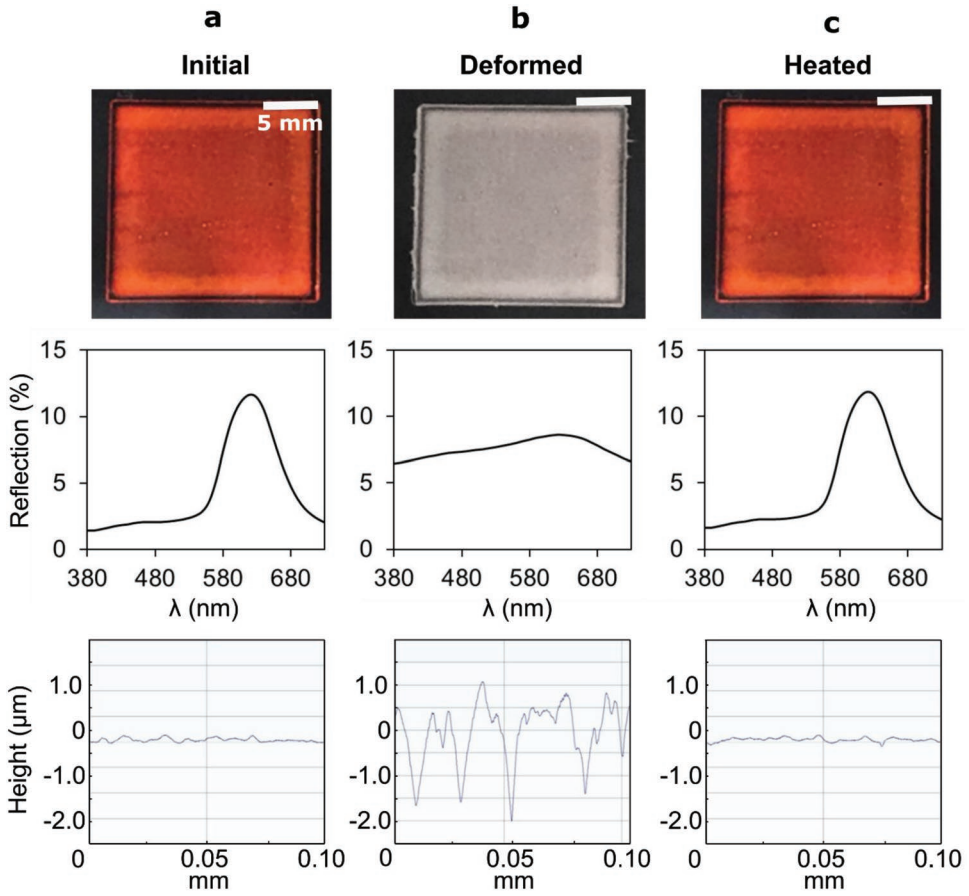

Figure 2. Photographs, reflection spectra, and height profiles of labels a) prior to deformation, b) after deformation by compression, and c) after subsequent heating. Scale bar = 5 mm. Reflection spectra were obtained using a colorimeter. Height profiles were obtained using a profilometer.

cylinder, spread evenly using a doctor blade, transferred to a printing cylinder containing 2 × 2 cm fields (full-tone), and subsequently transferred to the substrate thereby producing the coating. A black biaxially oriented polyethylene terephthalate (PET) substrate was selected to facilitate viewing of the structural color. After printing, the solvent was quickly evaporated at elevated temperature (70 °C), and the coating was briefly held at room temperature, which led to development of the CLC phase, and the appearance of a red reflection. The coatings were then photopolymerized by passing through a UV dryer in air, resulting in nonsticky and highly flexible polymeric PC coatings with a bright iridescent color. Upon normal (perpendicular) viewing, the coatings displayed a red reflection (**Figure 2**a) which was marked by a reflection band centered at 620 nm (Figure S2, Supporting Information). The surface roughness and thickness of the coatings were ≈0.02 and 3 μm, respectively, as measured by profilometry. The mid-point of the T_g was determined by DSC to be 18 °C, close to room temperature (Figure S3, Supporting Information).

Thermomechanical programming was performed by compressing the CLC coating into a rubberized metal sheet using a custom hot-stamp tool (Figure 1c; Figure S4, Supporting Information). The rubberized sheet had an arithmetic roughness (R_a) of ≈1 μm (Figure S5, Supporting Information). The temperature was set at 35 °C, which was chosen to be sufficiently above the T_g of the coating to induce the shape memory effect, but not so much as to cause irreversible plastic deformation. Compression below the T_g had no noticeable effect. After compression, the stamp was quickly removed thereby quenching the coating to room temperature, and the coating was peeled off of the rubberized sheet. Inspection of the deformed coating revealed a uniform matte gray appearance across the coating dimensions (2 × 2 cm) which was marked by a contrasting reflectivity spectrum (Figure 2b). The reflection at 620 nm is reduced, and the reflection at initially nonreflective wavelengths is significantly increased when compared with the initial state. As such, the reflection at all visible wavelengths is approximately equal, in agreement with the gray visual appearance of the coating as a result of the deformation. Investigation of the surface topography by profilometry revealed that the surface height profile is significantly altered from relatively smooth (R_a = 0.02 μm) to rough (R_a = 0.3 μm) as a result of the compression by the rough stamp (Figure 2b). Surface scattering is therefore identified as the primary source of the optical contrast. In fact, application of the same deformation protocol to a CLC coating in which the reflection band was shifted out of the visible range induced a similar optical effect (gray color; Figure S6, Supporting Information). Interestingly, the presence of a particle contamination had no effect on the deformation (Figure S7, Supporting Information).

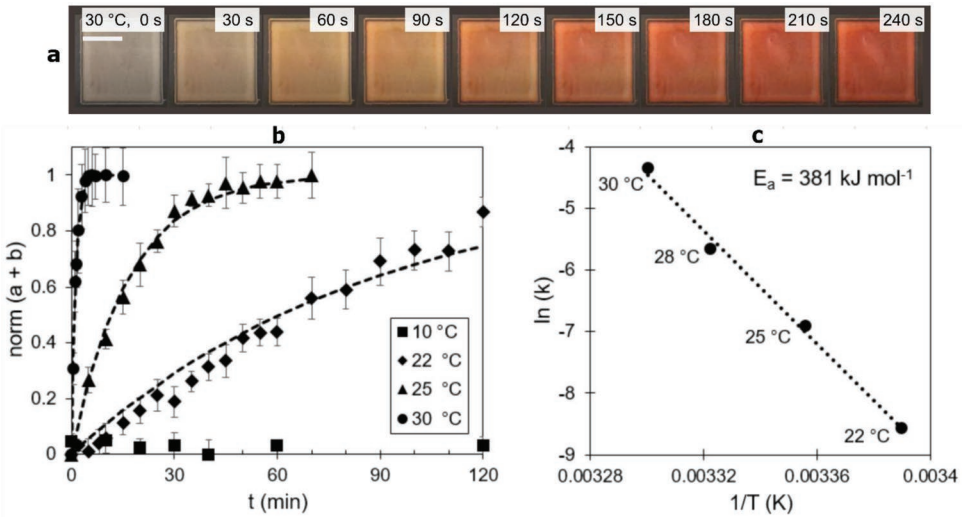

Figure 3. a) Time lapse photographs of an optical sensor held isothermally at 30 °C. The storage time is indicated in the top right of each frame. Scale bar = 1 cm. b) Color change over time during isothermal storage, plotted as normalized ($a + b$) values where "a" and "b" are the color axes in the CIELab color space. The error bars indicate the standard variation across three independent measurements. The dashed lines correspond to the fitted exponential decay functions. c) Arrhenius plot and derived activation energy for the measurement range 22–30 °C. The dashed line represents the line of best fit.

Briefly heating the deformed coating above the T_g (30 s, 40 °C) restored the initial red appearance of the coating, and completely returned the reflection spectrum back to the initial state (Figure 2c). At the same time, the surface topography was restored completely to its smooth initial state (R_a = 0.02 µm), indicating that the perceived optical change of the shape memory photonic coating is caused by the shape recovery from the deformed geometry to the initial geometry upon heating above T_g. We found that the low crosslinking density of the chiral nematic polymer network (consisting of 10% difunctional monomers) was critical for achieving the desired combination of mechanical deformation across the entirety of the coating thickness, and the remarkable ability to nevertheless make a complete recovery from the deformed state. Polymer networks containing a high amount of crosslinker (>20% difunctional monomers) were brittle in nature and prone to breakage upon deformation,[58] while those containing a low amount of crosslinker were tacky (<5% difunctional monomers). Using the chosen amount of crosslinker (10% difunctional monomers), the programming and recovery could be performed multiple times (>10), without significant loss of optical contrast (Figure S8, Supporting Information).

We found that the rate of the optical (and surface topographical) response of the deformed coating was highly temperature dependent. When stored at 10 °C ($T < T_{g,\ onset}$), no color change was observed to occur in the space of several months. When stored at 30 °C ($T > T_{g,\ end}$), a complete recovery was observed within ≈3 min (**Figure 3**a), while at 25 °C ($T = T_{g,\ end}$), the recovery took ≈1 h. This finding further demonstrates that the kinetics of the photonic response are related to the physical shape recovery[34,59] dependent on polymer chain mobility around the T_g.[2,64]

We further investigated the temperature dependence of the photonic response near T_g by measuring the color change under isothermal conditions using reflective colorimetry (see the Experimental Section). In Figure 3b, the onset of color over time is described by the normalized sum of the chromacity coordinates a and b in the CIELab color space. In each case, the optical response was fitted using an exponential decay function, according to

$$\text{norm}\ (a+b) = 1 - e^{-kt} \tag{1}$$

where k is the rate constant and t is the time. By plotting the rate constants over the measured range in an Arrhenius plot (Figure 3c, R^2 = 0.994 and standard deviation = 0.170), the activation energy was estimated to be ≈350–400 kJ mol^{-1}, which corresponds loosely to our previous reports of embossed CLC polymer networks,[59] and glassy polymers in general.[65,66]

3. Conclusions and Outlook

Thermoresponsive photonic coatings are fabricated that change both topography and color by exploiting the shape memory behavior of mechanically deformed chiral nematic polymer networks. Upon heating above room temperature, the coatings exhibit a distinct color change from matte gray to iridescent red with a high activation energy (350–400 kJ mol^{-1}) and therefore show a strong temperature dependence. Based on the extracted kinetic parameters, the current system is interesting for biomedical applications (i.e., fast optical switching at body temperature), or alternatively for cold-chain management applications (i.e., optical switching to indicate a temperature breach). Encouragingly, preliminary experiments show that small variations in the current ink formulation can be used to modify the response temperature to meet specific application specifications (Figure S9, Supporting Information). In principle, our method allows for the creation of temporary, arbitrary surface topographies by using the appropriate imprinted polymer stamp.

We also found that the presence of photonic structure is not a strict necessity for the generation of optical contrast,

suggesting that other shape memory materials could be used to generate irreversible thermoresponsive coatings based on this principle.[26,28,67,68] The thermoresponsive shape memory photonic coatings based on cholesteric polymer networks have a marginal cost due to the limited material required for their fabrication, and a low total production cost due to compatibility with the scalable and economic fabrication protocol of high-speed flexographic printing. The deformation protocol is robust, being insensitive to particle contamination or other irregularities in the CLC layer, and the use of a flexible rubber stamp circumvents planarization issues.[34,58,59] While currently plate-to-plate, the deformation protocol can also be envisioned in high-speed roll-to-roll or roll-to-plate processes,[69] for example, using a rubberized metal roll. Therefore, these thermoresponsive photonic coatings are promising for a wide range of low cost smart adhesives, adaptive biosurface, and optical sensor and devices.

4. Experimental Section

Materials: 2-methyl-1,4-phenylene bis(4-(((4-(acryloyloxy)butoxy) carbonyl)oxy)benzoate) **1** and (3R,3aS,6R,6aS)-hexahydrofuro[3,2-*b*] furan-3,6-diyl bis(4-((4-(((4-(acryloyloxy)butoxy)carbonyl)oxy)benzoyl) oxy)benzoate) **4** were obtained from BASF.

4-((6-(acryloyloxy)hexyl)oxy)phenyl 4-methoxybenzoate **2** was purchased from Synthon Chemicals. 4-cyanophenyl 4-((6-(acryloyloxy) hexyl)oxy)benzoate **3** was obtained from Merck. 2,2′-(ethane-1,2-diylbis(oxy))bis(ethane-1-thiol) **6** was purchased from Sigma-Aldrich. The photoinitiator 2-benzyl-2-(dimethylamino)-1-(4-morpholinophenyl) butan-1-one **5** was obtained from IGM resins. Cyclopentanone was purchased from Acros.

Preparation of Ink: The chiral nematic liquid crystal mixture contained 10% w/w of difunctional monomers, 84% of monofunctional monomers, 3% of dithiol, and 3% of photoinitiator. A small amount (0.1 wt%) of surfactant BYK-361 N (obtained from BYK) was also added. These components were dissolved in cyclopentanone (2:1 solids:solvent ratio), and the resulting solutions were filtered through a 0.2 µm PTFE syringe filter.

Preparation of Coatings: Coatings were prepared on an IGT printability tester F1 from IGT Testing System Pte Ltd., operating in flexo mode at 0.3 m s^{-1}. Biaxially oriented PET (Tenolan OCN0003, 36 µm thickness) was used as substrate. After coating, the coatings were heated to 70 °C for 30 s to evaporate the solvent, and annealed for 60 s at room temperature to align the CLC phase. Photopolymerization was performed by passing the substrate through an IGT UV Dryer in air (intensity: 155 mW cm^{-2} (UVA); 134 mW cm^{-2} (UVB), dose: 88 mJ cm^{-2} (UVA); 73 mJ cm^{-2} (UVB)). Finally, the coatings were heated to 70 °C for 30 s to ensure complete conversion of reactive acrylates, which was confirmed using Fourier transform infrared spectroscopy (FTIR) (Figure S10, Supporting Information).

Activation Protocol: A modified hot-stamp machine from KBA-Metronic GmbH was used to compress the surface of the coating into a rubberized metal sheet (Ra ≈ 1 µm) for 30 s at a pressure of 4.5 bar. The machine was fitted with a brass stamp heated to 35 °C. Following the compression, the coating was quickly returned to room temperature, removed from the machine, and stored in the fridge to avoid a premature color change.

Characterization: Polarized optical microscopy was performed with crossed polarizers using a Leica DM6000M equipped with a DFC420C camera and a Linkam THMS600 hot-stage for temperature control. Phase transition temperatures of the CLC mixtures and polymeric coatings were determined using a TA Instrument Q1000 differential scanning calorimeter (gas environment in the chamber was N_2). 3–4 mg of material was hermetically sealed (in air) in aluminum pans. The heating and cooling rate was 10 °C min^{-1}. For the monomer mixtures, the second cooling curve was used to determine the transition temperature. For the polymers, the second heating curve was used. Fourier transform infrared spectroscopy spectra were obtained using a Varian 3100 FT-IR equipped with a Golden gate diamond ATR and were signal-averaged over 50 scans at a resolution of 1 cm^{-1}. Profilometry experiments were performed using a Bruker DektakXT, set to measurement range 65.5 µm and stylus force 3 mg. The arithmetic average roughness R_a was calculated by the formula

$$R_a = \frac{1}{n}\sum_{i=1}^{n}|y_i| \tag{2}$$

where n is the number of measurements and y is the vertical deviation from the mean, according to DIN 4768/1.

Kinetic measurements were performed by placing three samples on an IKA RCT basic hotplate held isothermally. The temperature was calibrated using a Comark KM340 industrial thermometer. Reflectivity spectra and colorimetric data were obtained using an i1 Pro from X-Rite Inc. and a PerkinElmer Lambda 750 UV/vis/NIR spectrophotometer. The color change was described according to

$$\text{norm}\ (a+b) = \frac{(a+b)-(a+b)_{\min}}{(a+b)_{\max}-(a+b)_{\min}} \tag{3}$$

where norm $(a + b)$ represents the normalized color of the coating between compressed and heated states, a and b are the measured chromacity coordinates in the CIELab color space, and $(a + b)_{min}$ and $(a + b)_{max}$ are the minimum and maximum sum of the measured a and b parameters, respectively.

Supporting Information

Supporting Information is available from the Wiley Online Library or from the author.

Acknowledgements

The authors would like to thank Y. Foelen and M. D. T. Claessen for insightful discussions and helping with the repeatability experiments.

Conflict of Interest

The authors declare no conflict of interest.

Keywords

chiral nematic, cholesteric, liquid crystals, photonic crystals, sensors, shape memory, thermoresponsive

Received: April 10, 2019
Revised: May 21, 2019
Published online: June 19, 2019

[1] M. Behl, M. Y. Razzaq, A. Lendlein, *Adv. Mater.* **2010**, *22*, 3388.
[2] M. Behl, A. Lendlein, *Mater. Today* **2007**, *10*, 20.
[3] Y.-J. Kim, Y. T. Matsunaga, *J. Mater. Chem. B* **2017**, *5*, 4307.
[4] B. Q. Y. Chan, Z. W. K. Low, S. J. W. Heng, S. Y. Chan, C. Owh, X. J. Loh, *ACS Appl. Mater. Interfaces* **2016**, *8*, 10070.

[5] M. Ebara, *Sci. Technol. Adv. Mater.* **2015**, *16*, 014804.
[6] L. Zhao, L. Zhang, J. Zhao, J. Shi, Z. Dai, G. Wang, C. Zhang, B. Li, X. Feng, H. Zhang, J. Zhang, Z. Zhang, *ACS Appl. Mater. Interfaces* **2019**, *11*, 1563.
[7] Y. Zhang, Y.-T. Cheng, D. S. Grummon, *Appl. Phys. Lett.* **2006**, *89*, 041912.
[8] C.-C. Fu, A. Grimes, M. Long, C. G. L. Ferri, B. D. Rich, S. Ghosh, S. Ghosh, L. P. Lee, A. Gopinathan, M. Khine, *Adv. Mater.* **2009**, *21*, 4472.
[9] K. A. Burke, P. T. Mather, *J. Mater. Chem.* **2010**, *20*, 3449.
[10] M. Ebara, K. Uto, N. Idota, J. M. Hoffman, T. Aoyagi, *Adv. Mater.* **2012**, *24*, 273.
[11] J. D. Eisenhaure, T. Xie, S. Varghese, S. Kim, *ACS Appl. Mater. Interfaces* **2013**, *5*, 7714.
[12] Y. Wang, H. Lai, Z. Cheng, H. Zhang, Y. Liu, L. Jiang, *ACS Appl. Mater. Interfaces* **2019**, *11*, 10988.
[13] D. Zhang, Z. Cheng, Y. Liu, *Chem. - Eur. J.* **2019**, *25*, 3979.
[14] D. M. Le, K. Kulangara, A. F. Adler, K. W. Leong, V. S. Ashby, *Adv. Mater.* **2011**, *23*, 3278.
[15] T. Gong, K. Zhao, G. Yang, J. Li, H. Chen, Y. Chen, S. Zhou, *Adv. Healthcare Mater.* **2014**, *3*, 1608.
[16] S. Schauer, R. Schmager, R. Hünig, K. Ding, U. W. Paetzold, U. Lemmer, M. Worgull, H. Hölscher, G. Gomard, *Opt. Mater. Express* **2018**, *8*, 184.
[17] E. P. A. van Heeswijk, A. J. J. Kragt, N. Grossiord, A. P. H. J. Schenning, *Chem. Commun.* **2019**, *55*, 2880.
[18] J. Hou, M. Li, Y. Song, *Nano Today* **2018**, *22*, 132.
[19] D. Liu, D. J. Broer, *Soft Matter* **2014**, *10*, 7952.
[20] S. Schauer, M. Worgull, H. Hölscher, *Soft Matter* **2017**, *13*, 4328.
[21] Y. Ni, Y. Zhang, S.-Y. Leo, Y. Fang, M. Zhao, L. Yu, K. D. Schulze, W. G. Sawyer, T. E. Angelini, P. Jiang, C. R. Taylor, *ACS Appl. Nano Mater.* **2018**, *1*, 6081.
[22] J. Li, Y. An, R. Huang, H. Jiang, T. Xie, *ACS Appl. Mater. Interfaces* **2012**, *4*, 598.
[23] T. Xie, X. Xiao, J. Li, R. Wang, *Adv. Mater.* **2010**, *22*, 4390.
[24] Z. Wang, C. Hansen, Q. Ge, S. H. Maruf, D. U. Ahn, H. J. Qi, Y. Ding, *Adv. Mater.* **2011**, *23*, 3669.
[25] N. Schneider, C. Zeiger, A. Kolew, M. Schneider, J. Leuthold, H. Hölscher, M. Worgull, *Opt. Mater. Express* **2014**, *4*, 1895.
[26] H. Xu, C. Yu, S. Wang, V. Malyarchuk, T. Xie, J. A. Rogers, *Adv. Funct. Mater.* **2013**, *23*, 3299.
[27] A. Espinha, M. C. Serrano, Á. Blanco, C. López, *Adv. Opt. Mater.* **2014**, *2*, 516.
[28] C. López, *Adv. Mater.* **2003**, *15*, 1679.
[29] Y. Yin, J. Ge, *J. Mater. Chem. C* **2013**, *1*, 6001.
[30] C. G. Schäfer, M. Gallei, J. T. Zahn, J. Engelhardt, G. P. Hellmann, M. Rehahn, *Chem. Mater.* **2013**, *25*, 2309.
[31] C. G. Schäfer, D. A. Smolin, G. P. Hellmann, M. Gallei, *Langmuir* **2013**, *29*, 11275.
[32] C. G. Schäfer, C. Lederle, K. Zentel, B. Stühn, M. Gallei, *Macromol. Rapid Commun.* **2014**, *35*, 1852.
[33] Y. Fang, S.-Y. Leo, Y. Ni, L. Yu, P. Qi, B. Wang, V. Basile, C. Taylor, P. Jiang, *Adv. Opt. Mater.* **2015**, *3*, 1509.
[34] Y. Fang, Y. Ni, S.-Y. Leo, C. Taylor, V. Basile, P. Jiang, *Nat. Commun.* **2015**, *6*, 7416.
[35] Y. Fang, Y. Ni, S.-Y. Leo, B. Wang, V. Basile, C. Taylor, P. Jiang, *ACS Appl. Mater. Interfaces* **2015**, *7*, 23650.
[36] W. Niu, L. Qu, R. Lyv, S. Zhang, *RSC Adv.* **2017**, *7*, 22461.
[37] Y. Fang, S.-Y. Leo, Y. Ni, J. Wang, B. Wang, L. Yu, Z. Dong, Y. Dai, V. Basile, C. Taylor, P. Jiang, *ACS Appl. Mater. Interfaces* **2017**, *9*, 5457.
[38] C. J. Leverant, S.-Y. Leo, M. A. Cordoba, Y. Zhang, N. Charpota, C. Taylor, P. Jiang, *ACS Appl. Polym. Mater.* **2019**, *1*, 36.
[39] S.-Y. Leo, W. Zhang, Y. Zhang, Y. Ni, H. Jiang, C. Jones, P. Jiang, V. Basile, C. Taylor, *Small* **2018**, *14*, 1703515.
[40] A. J. J. Kragt, D. J. Broer, A. P. H. J. Schenning, *Adv. Funct. Mater.* **2018**, *28*, 1704756.
[41] J. Lub, V. Recaj, L. Puig, P. Forcén, C. Luengo, *Liq. Cryst.* **2004**, *31*, 1627.
[42] D. J. Broer, J. Boven, G. N. Mol, G. Challa, *Makromol. Chem.* **1989**, *190*, 2255.
[43] J. Lub, D. Broer, *Cross-Linked Liquid Crystalline Systems, Liquid Crystals Book Series*, CRC Press, Boca Raton, FL **2011**, pp. 3–47.
[44] I. Dierking, *Adv. Mater.* **2000**, *12*, 167.
[45] H. Shahsavan, S. M. Salili, A. Jákli, B. Zhao, *Adv. Mater.* **2015**, *27*, 6828.
[46] X. D. Feng, M. E. Tousley, M. G. Cowan, B. R. Wiesenauer, S. Nejati, Y. Choo, R. D. Noble, M. Elimelech, D. L. Gin, C. O. Osuji, *ACS Nano* **2014**, *8*, 11977.
[47] C. L. Gonzalez, C. W. M. Bastiaansen, J. Lub, J. Loos, K. Lu, H. J. Wondergem, D. J. Broer, *Adv. Mater.* **2008**, *20*, 1246.
[48] H. P. C. van Kuringen, G. M. Eikelboom, I. K. Shishmanova, D. J. Broer, A. P. H. J. Schenning, *Adv. Funct. Mater.* **2014**, *24*, 5045.
[49] S. J. Woltman, G. D. Jay, G. P. Crawford, *Nat. Mater.* **2007**, *6*, 929.
[50] J. Lub, D. J. Broer, R. A. M. Hikmet, K. G. J. Nierop, *Liq. Cryst.* **1995**, *18*, 319.
[51] Q. Li, *Intelligent Stimuli-Responsive Materials: From Well-Defined Nanostructures to Applications*, 1st ed., Wiley, New York **2013**.
[52] N. Herzer, H. Guneysu, D. J. D. Davies, D. Yildirim, A. R. Vaccaro, D. J. Broer, C. W. M. Bastiaansen, A. P. H. J. Schenning, *J. Am. Chem. Soc.* **2012**, *134*, 7608.
[53] D. J. Mulder, A. P. H. J. Schenning, C. W. M. Bastiaansen, *J. Mater. Chem. C* **2014**, *2*, 6695.
[54] D. J. Broer, C. M. W. Bastiaansen, M. G. Debije, A. P. H. J. Schenning, *Angew. Chem., Int. Ed.* **2012**, *51*, 7102.
[55] J. E. Stumpel, D. J. Broer, A. P. H. J. Schenning, *Chem. Commun.* **2014**, *50*, 15839.
[56] P. Zhang, A. J. J. Kragt, A. P. H. J. Schenning, L. T. de Haan, G. Zhou, *J. Mater. Chem. C* **2018**, *6*, 7184.
[57] E. P. A. van Heeswijk, J. J. H. Kloos, N. Grossiord, A. P. H. J. Schenning, *J. Mater. Chem. A* **2019**, *7*, 6113.
[58] D. J. D. Davies, A. R. Vaccaro, S. M. Morris, N. Herzer, A. P. H. J. Schenning, C. W. M. Bastiaansen, *Adv. Funct. Mater.* **2013**, *23*, 2723.
[59] M. Moirangthem, T. A. P. Engels, J. Murphy, C. W. M. Bastiaansen, A. P. H. J. Schenning, *ACS Appl. Mater. Interfaces* **2017**, *9*, 32161.
[60] A. K. O'Brien, N. B. Cramer, C. N. Bowman, *J. Polym. Sci., Part A: Polym. Chem.* **2006**, *44*, 2007.
[61] N. P. Godman, B. A. Kowalski, A. D. Auguste, H. Koerner, T. J. White, *ACS Macro Lett.* **2017**, *6*, 1290.
[62] D. C. Hoekstra, K. Nickmans, J. Lub, M. G. Debije, A. P. H. J. Schenning, *ACS Appl. Mater. Interfaces* **2019**, *11*, 7423.
[63] Y. Kimura, K. Kuboyama, T. Ougizawa, *Liq. Cryst.* **2016**, *43*, 587.
[64] V. Srivastava, S. A. Chester, L. Anand, *J. Mech. Phys. Solids* **2010**, *58*, 1100.
[65] M. L. Williams, R. F. Landel, J. D. Ferry, *J. Am. Chem. Soc.* **1955**, *77*, 3701.
[66] S. Vyazovkin, N. Sbirrazzuoli, I. Dranca, *Macromol. Chem. Phys.* **2006**, *207*, 1126.
[67] J. H. Park, H. Kim, J. R. Youn, Y. S. Song, *Smart Mater. Struct.* **2017**, *26*, 085026.
[68] Y. Gao, W. Liu, S. Zhu, *ACS Appl. Mater. Interfaces* **2017**, *9*, 4882.
[69] L. Peng, Y. Deng, P. Yi, X. Lai, *J. Micromech. Microeng.* **2014**, *24*, 013001.